09,04

Evolution of the spectral and structural characteristics of borates formed during the interaction of lanthanum and indium oxides with a potassium tetraborate melt

© S.Z. Shmurak, V.V. Kedrov, A.P. Kiselev, T.N. Fursova, I.I. Zver'kova

Osipyan Institute of Solid State Physics RAS,
Chernogolovka, Russia

E-mail: fursova@issp.ac.ru, zverkova@issp.ac.ru

Received June 27, 2023
Revised June 27, 2023
Accepted June 28, 2023

The structure, morphology, IR spectra, as well as luminescence spectra and luminescence excitation spectra of europium-doped borates formed during the interaction of lanthanum and indium oxides with a potassium tetraborate melt at 970°C have been studied. With an increase in the In^{3+} concentration in the batch, a sequential change of the following structural states is observed: single-phase $LaBO_3$ aragonite, $LaBO_3$ aragonite + $InBO_3$ calcite, single-phase $InBO_3$ calcite. The correspondence between the structure and spectral characteristics of these compounds has been established. It is shown that indium and lanthanum orthoborates do not form joint solid solutions

Keywords: rare earth orthoborates, crystal structure, X-ray diffraction analysis, IR spectroscopy, luminescence spectra.

DOI: 10.61011/PSS.2023.08.56582.125

1. Introduction

Great attention to the study of borates of rare earth elements $ReBO_3$ (Re = Lu, Eu, Tb, Gd, La) and $ReMe_3(BO_3)_4$ (Re = La, Eu, Sm) (Me = Al, Sc) is associated with the possibility of their use as effective phosphors for color displays, X-ray phosphors, LED light sources, nonlinear crystals [1–7]. To enable these compounds to be used in practice, directional change of their spectral response is essential. One of the effective methods of directional change of the emission spectra of polymorphic phosphors is to change their structural state [8–12]. Luminescence spectra of various structural modifications of borates $Lu_{1-x}Re_xBO_3$:Eu (Re = Gd, Tb, Eu, Y) and $Lu_{1-x}In_xBO_3$:Eu are investigated in [10–15]. These compounds contain $LuBO_3$, $ReBO_3$ and $InBO_3$. Lutetium orthoborate has two stable structural modifications: vaterite, which is formed at $T = 750-850$°C, and calcite, which is formed at $T = 970-1100$°C. Orthoborates $ReBO_3$ (Re = Gd, Tb, Eu, Y) have the structure of vaterite, and $InBO_3$ has the structure of calcite [16–21].

The following structural modification sequence (SMS) is observed in orthoborate $Lu_{0.98-x}In_xEu_{0.02}BO_3$ synthesized at $T = 780$°C (the temperature of existence of low-temperature vaterite $LuBO_3$), with an increase of the concentration of In: vaterite → vaterite + calcite → calcite. These samples crystallize in the calcite structure at concentrations of In ≥ 10 at.% [15]. The following SMS is observed in compounds $Lu_{0.99-x}Re_xEu_{0.01}BO_3$ (Re = Eu, Gd, Tb, Y) synthesized at $T = 970$°C (the temperature of existence of the calcite phase $LuBO_3$) with an increase of the concentration of Re: calcite → calcite + vaterite → vaterite. Samples $Lu_{0.99-x}Re_xEu_{0.01}BO_3$ crystallize in the vaterite structure at concentrations $Re \geq 10-25$ at.% for different Re [11–14]. Two narrow bands with $\lambda_{max} = 589.8$ and 595.7 nm (electronic transition $^5D_0 \rightarrow {}^7F_1$) [8–15] are observed in luminescence spectra of samples $Lu_{0.98-x}In_xEu_{0.02}BO_3$ and $Lu_{0.99-x}Re_xEu_{0.01}BO_3$ having a calcite structure. The luminescence spectrum of the vaterite modification of these compounds contains three bands: in the wavelength range 588–596 nm ($^5D_0 \rightarrow {}^7F_1$), 608–613 and 624–632 nm ($^5D_0 \rightarrow {}^7F_2$) [6–13]. Therefore, the Eu^{3+} ions located in compounds having the structure of calcite and vaterite are characterized by orange and red luminescence, respectively.

The bands with $\lambda_{max} = 589.4$, 591 and 592.6 nm ($^5D_0 \rightarrow {}^7F_1$) have the greatest intensity in the luminescence spectrum of lanthanum orthoborate $LaBO_3$(Eu), which has the structure of aragonite (sp. gr. *Pnam*), [22–25].

It was shown for the first time in [26,27] that the band with $\lambda_{ex} = 469$ nm ($^7F_0 \rightarrow {}^5D_2$) in the luminescence excitation spectra (LES) and the band in the wavelength range 577–582 nm ($^5D_0 \rightarrow {}^7F_0$) in the luminescence spectra of $La_{0.99-x}Re_xEu_{0.01}BO_3$ (Re = Tb, Y) compounds can serve as indicators of the structural state of the sample. A band with $\lambda_{ex} = 469$ nm is observed in LES of samples having a vaterite structure, while it is not observed in samples with an aragonite structure. In LS, if the maximum of the band corresponding to transition $^5D_0 \rightarrow {}^7F_0$ occurs at wavelengths less than 580 nm, then the sample has an aragonite structure, if it occurs at λ greater than 580 nm, then the sample has a vaterite structure.

The structural and spectral characteristics of orthoborates $La_{0.99-x}Re_xEu_{0.01}BO_3$ (Re=Tb, Y), $La_{0.98-x}Lu_xEu_{0.02}BO_3$, $Pr_{0.99-x}Lu_xEu_{0.01}BO_3$ and $Lu_{0.99-x}Sm_xEu_{0.01}BO_3$ synthesized at $T = 970°C$ were studied in [22,26–29]. Compounds $LaBO_3$ and $PrBO_3$ have two structural modifications. The low-temperature phase of these compounds is the orthorhombic phase — aragonite (sp. gr. *Pnam*). At $T = 1488°C$ $LaBO_3$ passes into the high-temperature monoclinic phase (sp. gr. $P2_1/m$), and $PrBO_3$ at $T = 1500°C$ — in the triclinic phase (sp. gr. $P(-1)$) [30–35]. The low-temperature phase of $SmBO_3$ is a triclinic structure (sp. gr. $P(-1)$), and at a temperature of $T = 1065-1150°C$ (according to various studies) $SmBO_3$ has a vaterite structure ($P6_3/mmc$) [17,36–38].

It should be noted that La^{3+} ions in the aragonite structure are surrounded by nine oxygen ions, and boron ions have trigonal oxygen coordination [32–35]. The Lu^{3+} ions in the calcite structure, for example, in $LuBO_3$, are surrounded by six oxygen ions, and boron atoms have the same trigonal oxygen coordination as in aragonite — $(BO_3)^{3-}$ [39]. Sm^{3+} ions in the triclinic structure of $SmBO_3$ are surrounded by eight oxygen ions, and boron ions have trigonal oxygen coordination [36]. At the same time, Lu^{3+} ions are surrounded by eight oxygen ions in the vaterite structure, and three boron atoms with a tetrahedral oxygen environment form a group $(B_3O_9)^{9-}$ in the form of a three-dimensional ring [39–41].

The following structural modification sequence (SMS) is observed in compounds $La_{0.99-x}Re_xEu_{0.01}BO_3$ (Re = Tb, Y) synthesized at $T = 970°C$ (the temperature of existence of aragonite phases $LaBO_3$ and vaterite $ReBO_3$), with an increase in the concentration of Re: aragonite → aragonite + vaterite → vaterite [26,27]. At the same time, an unexpected sequence of alternating structural modifications is observed in the orthoborates $La_{0.98-x}Lu_xEu_{0.02}BO_3$ and $Pr_{0.99-x}Lu_xEu_{0.01}BO_3$ synthesized at $T = 970°C$ (the temperature of the existence of phases of aragonite $LaBO_3$ and $PrBO_3$, as well as calcite $LuBO_3$), at as the concentration of Lu^{3+} increases: aragonite → aragonite + vaterite → vaterite → vaterite + calcite → calcite [22,28].

A sequential change of three structural states is also observed in orthoborates $Lu_{0.99-x}Sm_xEu_{0.01}BO_3$ synthesized at $T = 970°C$ (the temperature of existence of the calcite phase $LuBO_3$ and the triclinic phase of $SmBO_3$), with an increase in the concentration of Sm^{3+}: calcite → calcite + vaterite → vaterite → vaterite + triclinic phase → triclinic phase [29].

Thus, with an increase in the concentration of Lu in orthoborates $Re_{1-x}Lu_xBO_3$(Eu) (Re = La, Pr) and Sm in $Lu_{1-x}Sm_xBO_3$(Eu) these compounds first form a vaterite phase from the aragonite and calcite phases which are equilibrium at the synthesis temperature and only then transit to a structure which is equilibrium at the synthesis temperature. It should be noted that the concentration range of Sm^{3+}, in which there is a phase of vaterite in the orthoborates $Lu_{0.99-x}Sm_xEu_{0.01}BO_3$ synthesized at 970°C, is very wide $0.3 \le x \le 0.95$, at the same time, the triclinic phase exists in a very narrow interval — $0.98 < x \le 1$ [29].

It is important to note that the transition to the final structural modification in the orthoborates $Lu_{1-x}Re_xBO_3$: Eu, (Re = Gd, Tb, Eu, Y) and $Lu_{1-x}In_xBO_3$ synthesized at 970°C occurs at concentrations of In ≥ 10 at.% and $Re \ge 10-25$ at.% (for different Re) [11–15]. At the same time, this process ends at $x \ge 0.8-0.98$ in the orthoborates $La_{0.99-x}Re_xEu_{0.01}BO_3$ (Re = Tb, Y), $La_{0.98-x}Lu_xEu_{0.02}BO_3$, $Pr_{0.99-x}Lu_xEu_{0.01}BO_3$ and $Lu_{0.99-x}Sm_xEu_{0.01}BO_3$, synthesized at $T = 970°C$ (for different Re) [22,26–29].

Solid solutions of $LaBO_3$ and borates of rare earth ions $ReBO_3$ (Re = Tb, Y, Sm, Lu) were studied in [22,26–29]. The study of solid solutions $LaBO_3$ and borates that are not lanthanides was of interest. Solid solutions $LaBO_3$ and borate $ScBO_3$ with the general formula $La_{0.99-x}Sc_xEu_{0.01}BO_3$ ($0 \le x \le 0.99$) were studied in work [42].

As is known, scandium orthoborate ($ScBO_3$) has one structural modification — calcite at a temperature of 970°C [17,19,43].

Paper [42] showed that three compounds such as lanthanum orthoborate $LaBO_3$, lanthanum-scandium borate $LaSc_3(BO_3)_4$, scandium orthoborate $ScBO_3$ are successively formed in borates $La_{0.99-x}Sc_xEu_{0.01}BO_3$ when the concentration of Sc^{3+} ions increases.

– At $0 \le x \le 0.26$, the samples are single-phase and have an orthorhombic structure $LaBO_3$, sp. gr. *Pnam* (aragonite). Luminescence spectra and IR spectra of microcrystals of these samples corresponding to the aragonite phase were measured.

– At $0.26 < x < 0.75$, the samples are two-phase — along with the structure of aragonite a trigonal structure is observed $LaSc_3(BO_3)_4$, sp. gr. *R32H* (hantite). The relative amount of huntite increases, and the relative amount of aragonite decreases with an increase of the concentration of Sc^{3+} ions. The bands characteristic of the structures of aragonite $La_{0.99}Eu_{0.01}BO_3$ and huntite $La_{99-x}Sc_3Eu_{0.01}(BO_3)_4$ are observed in the luminescence spectra and IR spectra.

– At $0.75 \le x \le 0.85$ lanthanum is observed–scandium borate $LaSc_3(BO_3)_4$. The luminescence spectra of Eu^{3+} ions in these samples contain bands with λ_{max} = 589.8, 595.7 m ($^5D_0 \rightarrow {}^7F_1$); 610.2, 613.8, 615.8 nm ($^5D_0 \rightarrow {}^7F_2$); 692.2, 697.4, 701.2 nm ($^5D_0 \rightarrow {}^7F_4$). The bands with λ_{max} = 613.8 and 615.8 nm have the highest intensity. Absorption bands 665, 717, 752, 775, 968, 1234, 1338 cm^{-1} are observed in the IR spectra of huntite.

– In the interval $0.85 < x \le 0.97$, the samples are two-phase consisting of $LaSc_3(BO_3)_4$ and calcite $ScBO_3$, sp. gr. *R3c*. The relative amount of calcite increases with an increase of the concentration of Sc^{3+} ions and the amount of huntite decreases. Luminescence spectra and IR spectra contain the bands specific to huntite and calcite modifications of these samples.

– At $0.97 < x \le 0.99$, the samples have the structure of calcite $ScBO_3$. The bands with λ_{max} = 589.6 and 596.2 nm ($^5D_0 \rightarrow {}^7F_1$) have the highest intensity in the luminescence

spectrum of the sample $Sc_{0.99}Eu_{0.01}BO_3$. Absorption bands 644, 752, 775, 1236 and 1279 cm^{-1} are observed in IR spectra.

Thus, a successive change of structural states is observed in $La_{0.99-x}Sc_xEu_{0.01}BO_3$ compounds, with an increase of the concentration of Sc^{3+} in the batch: aragonite $LaBO_3$ $(0 \le x \le 0.26) \rightarrow$ aragonite + huntite $LaSc_3(BO_4)_3$ $(0.26 < x < 0.75) \rightarrow$ huntite $(0.75 \le x \le 0.85) \rightarrow$ huntite + calcite $ScBO_3$ $(0.85 < x \le 0.97) \rightarrow$ calcite $(0.97 < x \le 0.99)$.

Compounds $La_{0.99-x}Sc_xEu_{0.01}BO_3$ have a high luminescence intensity and can be used as effective red phosphors for LED light sources.

The structure, IR spectra, morphology, luminescence spectra and luminescence excitation spectra in the system $LaBO_3-InBO_3$ are studied herein. Indium, unlike scandium, is not a rare earth element, it belongs to the IIIa group of elements and its ion In^{3+} has a larger radius. The phases formed in this system with an increase in the concentration of indium in the charge are determined in this paper. The correspondence between the structure and spectral characteristics of the synthesized compounds was established. Eu^{3+} ions, like in our previous studies, were used as optically active and structurally sensitive labels in quantities that do not affect the structural transformations of the studied compounds.

2. Experimental procedures

2.1. Sample synthesis

Samples of polycrystalline orthoborate powders with the gross formula $La_{0.99-x}In_xEu_{0.01}BO_3$ were synthesized at $0 \le x \le 0.99$ by the interaction of lanthanum, indium and europium oxides with a potassium tetraborate melt by reaction

$$(0.99 - x)La_2O_3 + xIn_2O_3 + 0.01Eu_2O_3 + K_2B_4O_7 = 2La_{0.99-x}In_xEu_{0.01}BO_3 + K_2B_2O_4.$$

The amount of potassium tetraborate taken into the reaction provided a twofold excess of the boron-containing reagent relative to the stoichiometric amount. The initial reagents for the synthesis were potassium tetraborate hydrate $K_2B_4O_7 \cdot 4H_2O$, metal oxides and nitric acid. All chemicals were of „analytical reagent grade". Metal ions were introduced into the reaction in the form of aqueous solutions of their nitrate salts, which were previously obtained by dissolving the initial metal oxides in nitric acid. Microcrystalline borate powders were synthesized as follows. Accurately weighed crystalline potassium tetraborate (hydrate) and appropriate volumes of calibrated aqueous solutions of rare earth nitrates were placed in a ceramic cup and mixed thoroughly. The obtained aqueous suspension was heated on a hot plate with water distilled off at a moderate boil. The resulting solid product was annealed at 550°C during 20 min to remove any residual moisture and to decompose the nitrate salts. The solid precursor product was carefully ground in an agate mortar and then the resulting powder was placed in a ceramic for annealing at $T = 970$°C during 3 h. The derived products were treated with 5 wt.% aqueous solution of hydrochloric acid during 0.2 h. Borate polycrystals were extracted by filtering the obtained aqueous suspension, followed by washing with water and alcohol and drying on the filter. The obtained polycrystal powders were finally air dried at $T = 120$°C during 0.5 h.

2.2. Research methods

X-ray diffraction studies were performed using a Rigaku SmartLab SE diffractometer with CuK_α-radiation, $\lambda = 1.54178$ Å, 40 kV, 35 mA. Angular spacing is $2\theta = 10-140°$. Phase analysis of the samples and calculation of lattice parameters were performed using Match and PowderCell 2.4 software.

The IR absorption spectra of the samples were measured on a VERTEX 80v Fourier spectrometer in the spectral range $400-5000\ cm^{-1}$ with a resolution of $2\ cm^{-1}$. For measurements, the polycrystal powders were ground in the agate mortar, and then applied in a thin layer onto a polished KBr crystalline substrate.

The sample morphology was examined using Supra 50VP X-ray microanalyzer with INCA EDS accessory (Oxford).

Photoluminescence spectra and luminescence excitation spectra were studied on a unit consisting of a light source — DKSSh-150 lamp, two MDR-4 and MDR-6 monochromators (spectral range 200–1000 nm, dispersion 1.3 nm/mm). Luminescence was recorded using photomultiplier FEU-106 (spectral sensitivity range 200–800 nm) and an amplification system. The MDR-4 monochromator was used to study the samples luminescence excitation spectra, the MDR-6 monochromator was used to study luminescence spectra. Spectral and structural characteristics as well as morphology of the samples were studied at room temperature.

Before proceeding to the presentation of the results of structural and spectral studies of the obtained samples of orthoborates, it is important to note that the gross formulas given in the text of the article are of the form $La_{0.99-x}In_xEu_{0.01}BO_3$ are not characteristics of individual compounds, and reflect only the ratio of atomic fractions of rare earth elements and indium in the initial batch.

3. X-ray diffraction studies

Diffractograms of powders of samples $La_{0.99-x}In_xEu_{0.01}BO_3$ and their phase composition depending on the concentration of indium in the batch are shown in Figs. 1 and 2. The samples are single-phase at $0 \le x \le 0.20$ and have the structure of aragonite $LaBO_3$, sp. gr. *Pnam* (62) (PDF 12-0762), $Z = 4$. The samples are two-phase in the interval of $0.20 < x < 0.94$ — along with the structure of aragonite, calcite $InBO_3$, etc. gr. $R\bar{3}c$

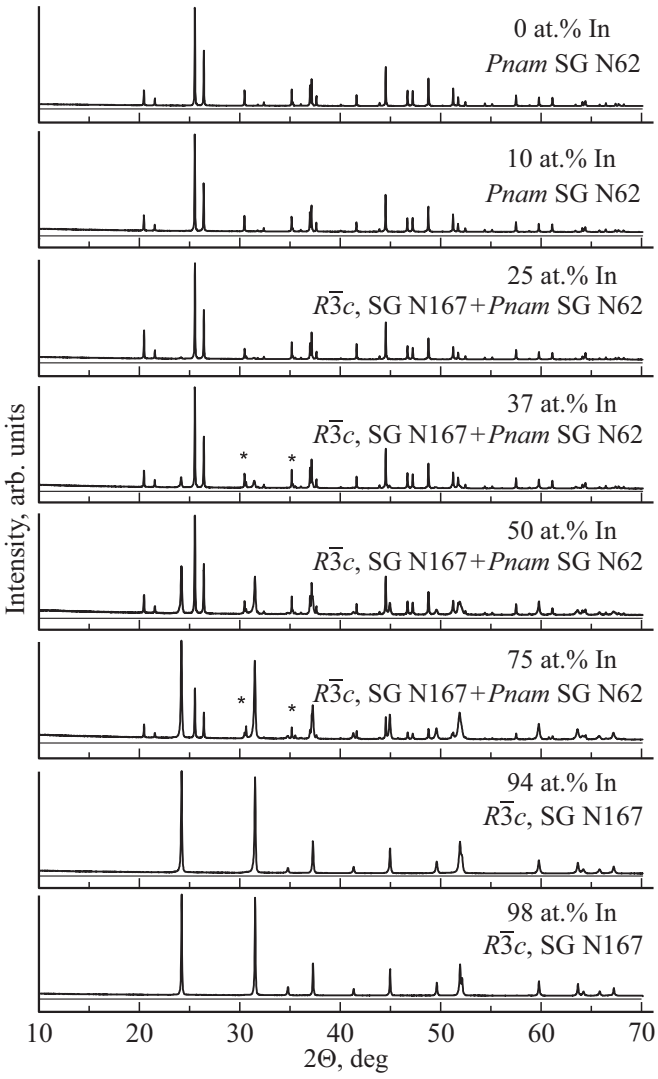

Figure 1. Diffractograms of samples $La_{0.99-x}In_xEu_{0.01}BO_3$ ($0 \le x \le 0.99$). * — In_2O_3.

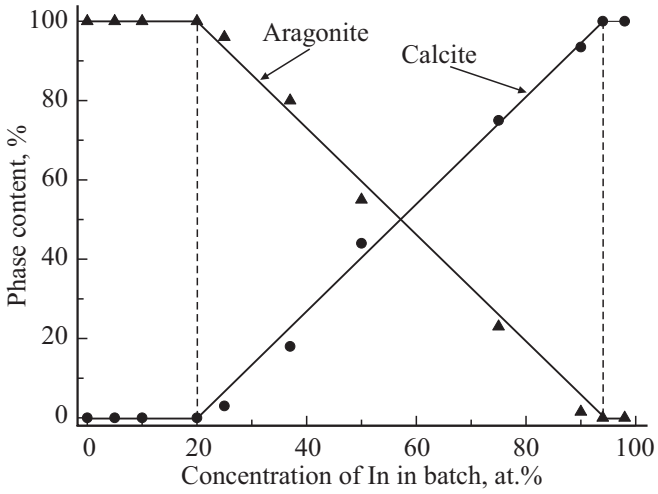

Figure 2. Phase composition of borates $La_{0.99-x}In_xEu_{0.01}BO_3$ depending on the concentration of indium in the batch at $0 \le x \le 0.99$: triangle — aragonite; circle — calcite.

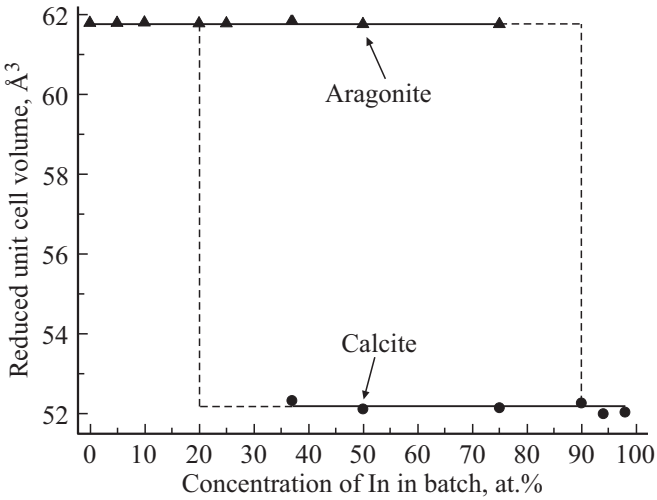

Figure 3. Unit cell volumes of aragonite and calcite, depending on the concentration of indium in the batch at $0 \le x \le 0.99$, reduced to the formula unit $(La,In)BO_3$: triangle — aragonite, circle — calcite.

(167), PDF 82-1188, $Z = 6$. The samples are single-phase at $0.94 \le x \le 0.99$, with a calcite structure $InBO_3$.

Figure 3 shows the unit cell volumes of the phases observed in borates $La_{0.99-x}In_xEu_{0.01}BO_3$, reduced to the formula unit $(La,In)BO_3$. Unit cell volume (V_A) does not change in the entire interval of the existence of the aragonite phase (Table, Fig. 3).

The ionic radius In^{3+} (0.84285 Å) is significantly smaller than the ionic radius La^{3+} (1.11482 Å) [44]. The absence of a change in the unit cell volume of the aragonite in the single-phase region $0 \le x \le 0.20$ indicates that indium ions are not included in the structure of aragonite. The actual content of lanthanum and indium in the samples, determined according to the data of elemental analysis, is given in the Table. It can be seen that the samples practically do not contain indium in the interval $0 \le x \le 0.20$. This means that the indium introduced into the batch in this synthesis method is washed out during the treatment of samples with acid and is not included in the structure of aragonite in the range $0 \le x \le 0.20$. The added indium in the interval $0.20 < x < 0.94$ forms the calcite phase, the amount of which increases and reaches 100% at $0.94 \le x \le 0.99$. Since the unit cell volume of aragonite does not change throughout the observation interval of this phase, this indicates that indium does not enter the aragonite lattice at $0 \le x < 0.94$. The unit cell volume of calcite is also practically constant in this interval, i.e. we do not observe doping of calcite $InBO_3$ with lanthanum. The unit cell volume also practically does not change with the increase of the concentration of indium in the batch in the narrow range of indium concentrations $0.94 \le x \le 0.99$, in which single-phase calcite $InBO_3$ is observed (Fig. 3, Table). In other words, the unit cell volume of calcite practically does not change when $InBO_3$ lanthanum with a larger ionic radius than the radius of the indium ion is added to calcite. Thus,

The content of phases, the reduced unit cell volume of calcite and aragonite, and the actual content of elements depending on the content of indium in the batch of $La_{0.99-x}In_xEu_{0.01}BO_3$

In, at.% in batch, x	Calcite, %	Aragonite, %	Reduced unit cell volume		Content In_2O_3 %	Actual quantity	
			calcite (: 6)	aragonite (: 4)		La, at %	In, at %
0*	0	100	–	61.79	–	100	0
5	0	100	–	61.80	–	99.5	0.5
10	0	100	–	61.81	–	100	0
20	< 1	> 99	–	61.79	–	99	1
25	3	96	–	61.79	1	96	4
37	15	85	52.33	61.81	2	85	15
50	44	55	52.12	61.77	1	51	49
75	75	23	52.15	61.77	2	24	76
90	93.5	1.5	52.27	–	5	5	95
94	100	–	52.00	–	–	2	98
98*	100	–	52.04	–	–	0	100

Comment. * — sample composition $La_{0.98-x}In_xEu_{0.02}BO_3$.

we do not observe the entry of lanthanum ions into the calcite crystal lattice.

The Table shows that the actual lanthanum content in the sample practically coincides with the concentration of the aragonite phase, and the actual indium content correlates with the amount of the calcite phase. This once again confirms the assumption that aragonite contains $LaBO_3$ without indium entering the crystal lattice, and the indium added during synthesis is consumed to form calcite $InBO_3$.

Based on X-ray diffraction studies of $La_{0.99-x}In_xEu_{0.01}BO_3$ compounds, it can be concluded that with an increase in the concentration of In^{3+} in the batch, a sequential change of the following structural states is observed: single-phase aragonite ($0 \le x \le 0.20$), aragonite + calcite ($0.20 < x < 0.94$), single-phase calcite ($0.94 \le x \le 0.98$).

4. Sample morphology

The microcrystals obtained at $T = 970°C$ $La_{0.98}Eu_{0.02}BO_3$ with an aragonite structure (Table) have dimensions of $\sim 1-6\,\mu$m (Fig. 4, *a*), are well-faceted and have a ratio of maximum to minimum size close to one. Samples $La_{0.99-x}In_xEu_{0.01}BO_3$ ($0 < x < 0.2$) also have an aragonite structure and similar morphology, for example, sample $La_{0.89}In_{0.10}Eu_{0.01}BO_3$ (Fig. 4, *b*). Sample $La_{0.62}In_{0.37}Eu_{0.01}BO_3$ (85% aragonite (A), 13% calcite (C) and 2% In_2O_3, Table) contains, along with the above polyhedral microcrystals, also small (mainly $< 1\,\mu$m) particles without a definite shape (Fig. 4, *c*). Noticeably more small particles with sizes $< 1\,\mu$m are observed with a higher indium content in the sample composed of $La_{0.49}In_{0.50}Eu_{0.01}BO_3$ (65% A, 44% C and 1% In_2O_3) and there are also individual rhombohedral microcrystals with sizes $\sim 1-2\,\mu$m (Fig. 4, *d*). The number of fine particles becomes even larger with a further increase of the indium concentration, for example, the sample $La_{0.24}In_{0.75}Eu_{0.01}BO_3$ (23% A, 75% C and 1% In_2O_3) (Fig. 4, *e*). The sample $In_{0.98}Eu_{0.02}BO_3$, which has a calcite structure (Table), consists mainly of microcrystals of size $\sim 1\,\mu$m and less (Fig. 4, *f*).

Based on the study of borate morphology $La_{0.98-x}In_xEu_{0.02}BO_3$ ($x = 0$ and $x = 0.98$) and $La_{0.99-x}In_xEu_{0.01}BO_3$ ($0 \le x \le 0.99$) it can be concluded that the dispersion of samples is the main difference between orthoborates $La_{0.98}Eu_{0.02}BO_3$ having the structure of aragonite, and orthoborates $In_{0.98}Eu_{0.02}BO_3$ having the structure of calcite, namely: the sizes of microcrystals $1-6\,\mu$m for aragonite (Fig. 4, *a*) and the sizes of microcrystals $\sim 1\,\mu$m and less for calcite (Fig. 4, *f*). Two-phase samples contain both particle fractions of different dispersion with quantities correlating with the ratio of lanthanum and indium.

5. Results of IR spectroscopy

Figure 5 shows the IR spectra of $La_{0.98-x}In_xEu_{0.02}BO_3$ compounds, where $x = 0, 0.98$ (spectra *1* and *8* respectively) and $La_{0.99-x}In_xEu_{0.01}BO_3$, where $x = 0.10$, 0.25, 0.37, 0.50, 0.75 and 0.94 (spectra *2–7*) in the frequency range $500-1500\,cm^{-1}$, characteristic of internal vibrations of the ion $(BO_3)^{3-}$. According to the data of X-ray phase analysis, the sample of $La_{0.98}Eu_{0.02}BO_3$ is single-phase and has the structure of aragonite (Table). Boron with three oxygen atoms form an ion $(BO_3)^{3-}$ with positional symmetry C_s in this structure. Intense absorption bands are observed in the IR absorption spectrum of $La_{0.98}Eu_{0.02}BO_3$ (Fig. 5, spectrum *1*) 592, 612, 721, 789, 939 and $1302\,cm^{-1}$. In accordance with the analysis of internal vibrations of this ion in the structure of aragonite [39], the IR absorption bands 592 and $613\,cm^{-1}$ can be attributed to the bending plane vibration ν_4, doublet 723, 789 — to the bending out-of-plane vibration ν_2, and the absorption bands 940 and $1306\,cm^{-1}$ — to the stretching

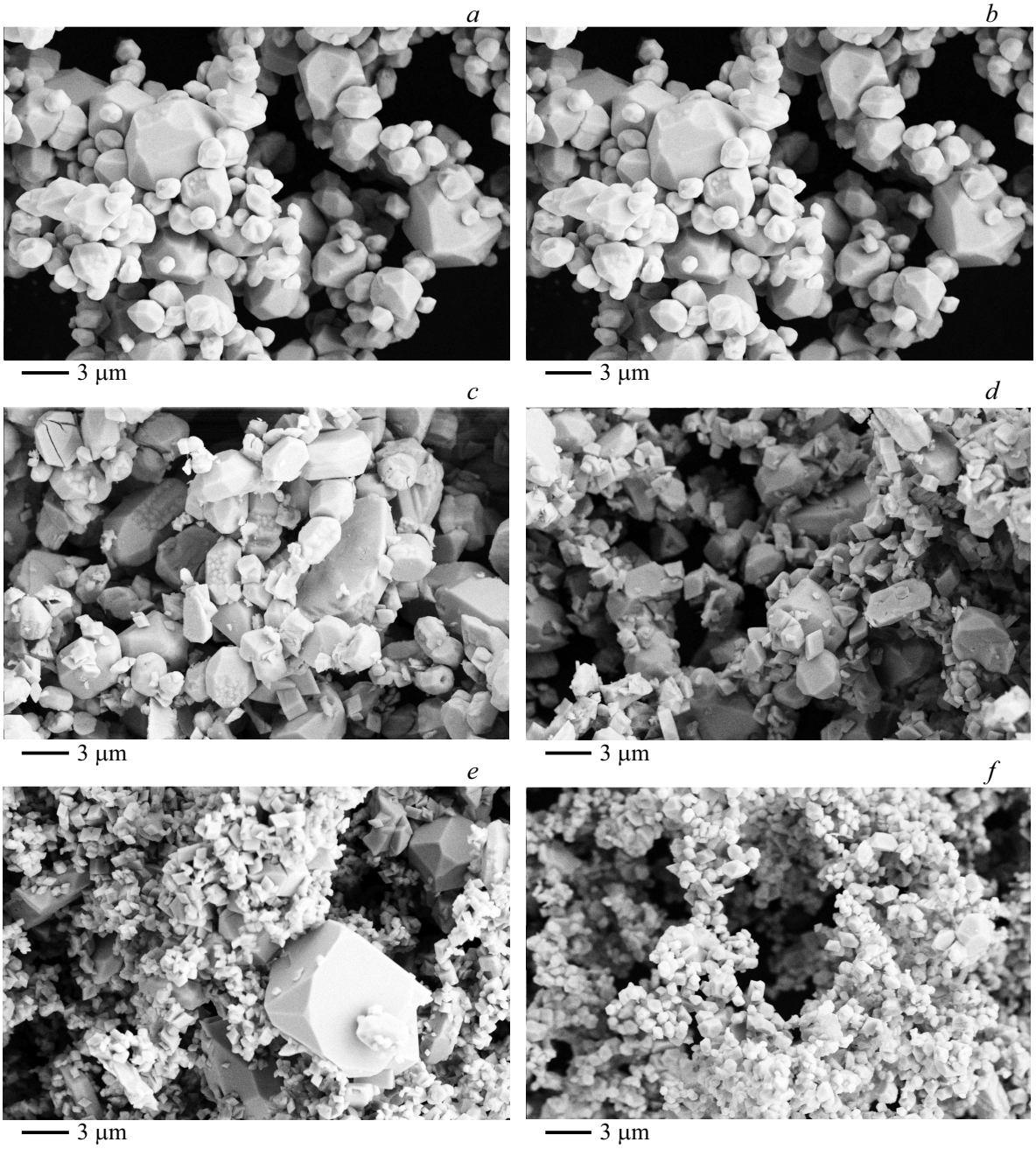

Figure 4. Morphology of borates $La_{0.99-x}In_xEu_{0.01}BO_3$ *a* — $La_{0.98}Eu_{0.02}BO_3$; *b* — $La_{0.89}In_{0.10}Eu_{0.01}BO_3$; *c* — $La_{0.62}In_{0.37}Eu_{0.01}BO_3$; *d* — $La_{0.49}In_{0.50}Eu_{0.01}BO_3$; *e* — $La_{0.24}In_{0.75}Eu_{0.01}BO_3$; *f* — $In_{0.98}Eu_{0.02}BO_3$.

symmetric ν_1 and antisymmetric ν_3 vibrations, respectively (fig. 5, spectrum *1*). Similar spectra were observed in [25,34,45]. The IR spectrum of $La_{0.89}In_{0.1}Eu_{0.01}BO_3$ has the same set of absorption bands, designated „a“, and is single-phase with the structure of aragonite according to the results of X-ray phase analysis (Table).

In spectra of samples $La_{0.99-x}In_xEu_{0.01}BO_3$ containing 25, 37, 50 and 75 at.% In^{3+}, along with the bands „a“, new bands appear, designated „c“ (Fig. 5, spectra *3*–*6*). These samples are two-phase — along with the aragonite phase $LaBO_3$, they contain the calcite phase $InBO_3$ (Table). The figure clearly shows the transformation of the absorption spectra of samples with increasing indium concentration: the intensity of the absorption bands of the aragonite phase decreases, and the absorption bands „c“ increases. The calcite/vaterite phase ratio in samples $La_{0.74}In_{0.25}Eu_{0.01}BO_3$, $La_{0.62}In_{0.37}Eu_{0.01}BO_3$, $La_{0.49}In_{0.50}Eu_{0.01}BO_3$ and $La_{0.24}In_{0.75}Eu_{0.01}BO_3$ is 3/96, 15/85, 44/55 and 75/23 respectively according to the results of X-ray phase analysis. Only absorption bands „c“ are observed in spectra of samples $La_{0.05}In_{0.94}Eu_{0.01}BO_3$ and $In_{0.98}Eu_{0.02}BO_3$ (Fig. 5, spectra *7, 8*). They are single-

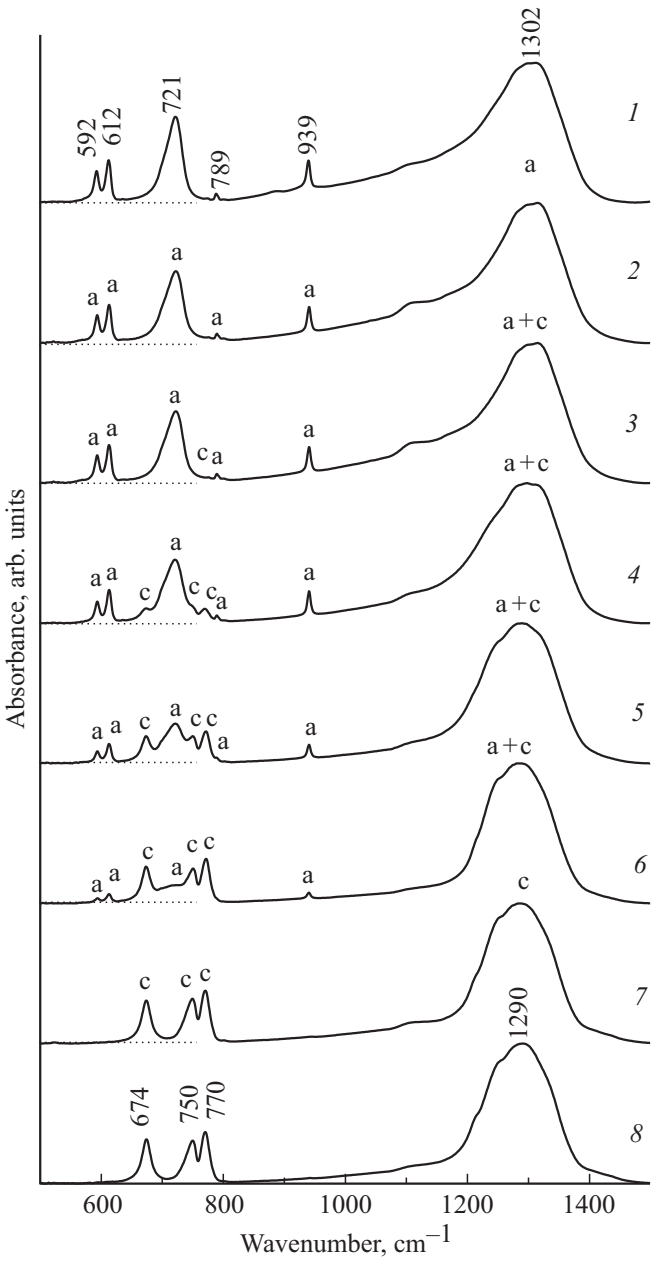

Figure 5. IR spectra of borates $La_{0.99-x}In_xEu_{0.01}BO_3$ *1* — $La_{0.98}Eu_{0.02}BO_3$; *2* — $La_{0.89}In_{0.1}Eu_{0.01}BO_3$; *3* — $La_{0.74}In_{0.25}Eu_{0.01}BO_3$; *4* — $La_{0.62}In_{0.37}Eu_{0.01}BO_3$; *5* — $La_{0.49}In_{0.5}Eu_{0.01}BO_3$; *6* — $La_{0.24}In_{0.75}Eu_{0.01}BO_3$; *7* — $La_{0.05}In_{0.94}Eu_{0.01}BO_3$; *8* — $In_{0.98}Eu_{0.02}BO_3$; The zero values of the ordinate axes are shown by a dotted line for spectra *1–8*.

phase with a calcite structure according to the results of X-ray phase analysis. The absorption bands 674, 750, 770 and 1290 cm^{-1} are observed in the spectra of these samples due to vibrations in the B-O bonds of the planar trigonal ion $(BO_3)^{3-}$ with positional symmetry D_3 (Fig. 5, spectrum *8*). A similar spectrum for $InBO_3$ was observed earlier in [39,45]. The band 674 and doublet 750 and 770 cm^{-1} are attributed to bending planar and out-of-plane vibrations of B-O bonds — ν_4 and ν_2, respectively, and the wide band 1290 — to the stretching asymmetric vibrations of these bonds.

Thus, the IR spectroscopy method shows that the IR absorption spectra of samples $La_{0.98}Eu_{0.02}BO_3$, $La_{0.89}In_{0.1}Eu_{0.01}BO_3$ and $La_{0.05}In_{0.94}Eu_{0.01}BO_3$, $In_{0.98}Eu_{0.02}BO_3$ correspond to the spectra of single-phase samples with aragonite and calcite structures, respectively, in which planar trigonal groups BO_3 are present. The difference in the spectra in the frequency range of the B-O bond vibrations is due to the different positional symmetry of the ion $(BO_3)^{3-}$: C_s — in the structure of aragonite and D_3 — in the structure of calcite. The samples of the gross compositions $La_{0.99-x}In_xEu_{0.01}BO_3$ $(0.20 < x < 0.94)$ are two-phase: their IR spectra include absorption bands of both the aragonite phase and calcite.

6. Spectral characteristics of borates $La_{0.99-x}In_xEu_{0.01}BO_3$

Samples $La_{0.99-x}In_xEu_{0.01}BO_3$ have the structure of aragonite $(0 \le x \le 0.20)$ in case of the increase of indium concentration in the batch and are single-phase according to the data of X-ray phase analysis (sec. 3). Then, the calcite phase is formed along with the aragonite phase $(0.20 < x < 0.94)$, and single-phase samples $In_{0.94}La_{0.05}Eu_{0.01}BO_3$ and $In_{0.98}Eu_{0.02}BO_3$ have a calcite structure at $0.94 \le x \le 0.98$. The luminescence spectra (LS) of these compounds are shown in Fig. 6. Bands with λ_{max} are observed in LS of single-phase samples $La_{0.94}In_{0.05}Eu_{0.01}BO_3$, $La_{0.89}In_{0.1}Eu_{0.01}BO_3$ and $La_{0.79}In_{0.2}Eu_{0.01}BO_3$ having an aragonite structure: 578.8 nm (2.142 eV) (electronic transition $^5D_0 \to {}^7F_0$); 589.5, 591.2, 592.8 nm (2.103, 2.097, 2.091 eV) ($^5D_0 \to {}^7F_1$); 611.6, 614.5, 617.4, 620, 623.2 nm (2.027, 2.017, 2.008, 1.999, 1.989 eV) ($^5D_0 \to {}^7F_2$) (Fig. 6, spectra *1–3*). The band with $\lambda_{max} = 614.5$ has the highest intensity in the given wavelength range. Similar spectra were observed in [22–25].

Figure 6 (spectra *8, 9*) shows LS of single-phase samples $In_{0.94}La_{0.05}Eu_{0.01}BO_3$ and $In_{0.98}Eu_{0.02}BO_3$ with calcite structure. Bands with $\lambda_{max} = 589.4$ and 596.5 nm (2.103 and 2.078 eV) ($^5D_0 \to {}^7F_1$) are observed in the spectra, the position of which is close to the position of bands in the calcite modification $LuBO_3$(Eu) [10–12].

Luminescence excitation spectra (LES) of the most intense luminescence bands of borates $La_{0.94}In_{0.05}Eu_{0.01}BO_3$ and $In_{0.98}Eu_{0.02}BO_3$ having the structure of aragonite and calcite, respectively, are shown in Fig. 7.

A wide band ($\lambda = 200-330$ nm) is observed in the ultraviolet region of the spectrum (charge transfer band — CTB) in LES $La_{0.94}In_{0.05}Eu_{0.01}BO_3$ (LBO), with a maximum at ~ 280 nm (Fig.7, spectrum *1*). The LES of this sample also contains a number of narrow bands in the wavelength range 330–500 nm corresponding to the resonant excitation of Eu^{3+} ions. The bands with maxima at $\lambda_{ex} = 394$ nm ($^7F_0 \to {}^5L_6$) and 465.5 nm ($^7F_0 \to {}^5D_2$) are the most intense

in the long-wavelength region of the spectrum for LBO. The luminescence excitation spectrum of the most intense luminescence band of the orthoborate $In_{0.98}Eu_{0.02}BO_3$ ($\lambda_{max} = 589.4$ nm) having a calcite structure (Table) is shown in Fig. 7, spectrum *2*. It contains a wide band 200–280 nm (CTB) with a maximum at $\lambda_{ex} \sim 242$ nm, and in the range 280–500 nm band $\lambda_{ex} = 394$ nm weak intensity (Fig. 7, spectrum *2*, insert).

The intensity of the luminescence bands of the calcite phase in two-phase samples (Fig. 6, spectra *4*–*7*) is small compared to the bands of the aragonite phase, despite the fact that according to X-ray phase analysis (Table), the amount of calcite phase in two-phase samples reaches 75%. The low intensity of the luminescence bands of calcite is due to the very low intensity of the excitation band with $\lambda_{ex} = 394$ nm in the LES (Fig. 7, spectrum *2*, insert). The intensity of the resonant excitation band of luminescence $\lambda_{ex} = 394$ nm in calcite is about an order of magnitude less than in aragonite (Fig. 7, spectrum *1*).

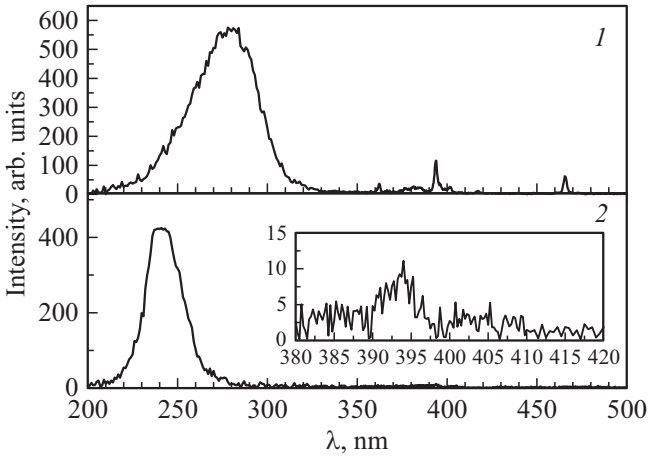

Figure 7. Luminescence excitation spectra of samples: *1* — $La_{0.94}In_{0.05}Eu_{0.01}BO_3$, *2* — $In_{0.98}Eu_{0.02}BO_3$ obtained at λ_{max}: *1* — 614.5 nm, *2* — 589.5 nm. The inset shows a section of the spectrum *2* in the wavelength range 380–420 nm.

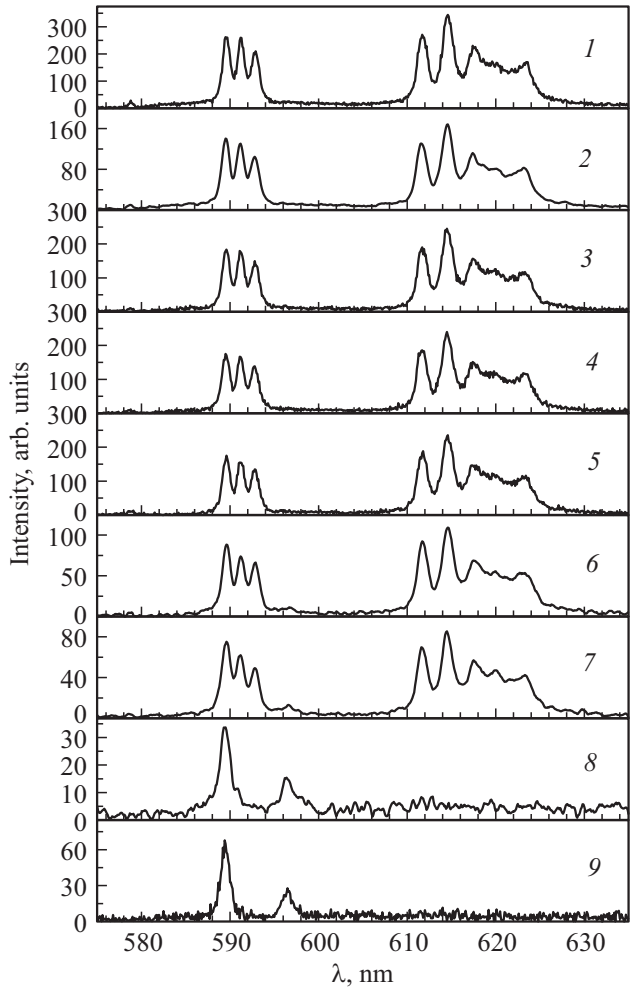

Figure 6. Luminescence spectra of borates $La_{0.99-x}In_xEu_{0.01}BO_3$ when excited by wavelength $\lambda_{ex} = 394$ nm. *1* — $x = 0.05$; *2* — $x = 0.1$; *3* — $x = 0.2$, *4* — $x = 0.25$; *5* — $x = 0.37$; *6* — $x = 0.5$; *7* — $x = 0.75$; *8* — $x = 0.94$; *9* — $In_{0.98}Eu_{0.02}BO_3$.

Thus, a comparison of the results of X-ray phase analysis and luminescence spectra indicates that there is a correspondence between the structure and spectral characteristics of orthoborates $La_{0.99-x}In_xEu_{0.01}BO_3$ at $0 \le x \le 0.99$.

7. Conclusion

The structure, morphology, IR spectra, as well as luminescence excitation spectra and luminescence spectra of lanthanum and indium orthoborates synthesized at 970°C with the general formula $La_{0.99-x}In_xEu_{0.01}BO_3$ were studied in this paper. An unambiguous correspondence was established between the structural modification of orthoborates, their IR spectra and photoluminescence spectra.

It was shown that solid solutions of lanthanum and indium orthoborates are not formed in the studied system, as evidenced by the constancy of the unit cell volume with an increase in the concentration of In^{3+} ions in the batch. At the same time, a successive batch of the following structural states is observed: single-phase aragonite $LaBO_3$ ($0 \le x \le 0.20$), aragonite + calcite $InBO_3$ ($0.20 < x < 0.94$), single-phase calcite ($0.94 \le x \le 0.98$).

– At $0 \le x \le 0.20$ the samples are single-phase and have the structure of aragonite $LaBO_3$ (sp. gr. *Pnam*).

– At $0.20 < x < 0.94$ the samples are two-phase contain aragonite and calcite. The relative amount of calcite increases, and aragonite decreases with an increase in the concentration of ions In^{3+} in the batch. The actual lanthanum content in the sample practically coincides with the concentration of the aragonite phase, and the actual indium content correlates with the amount of the calcite phase. I. e., the added indium forms the calcite phase and does not enter the aragonite lattice in the entire studied interval. The unit cell volume of calcite also does

not change. Bands characteristic of aragonite and calcite structures are observed in the luminescence and IR spectra.

– At $0.94 \leq x \leq 0.98$ the samples are single-phase with the structure of calcite $InBO_3$ (sp. gr. $R\bar{3}c$). The unit cell volume of calcite is almost constant, therefore, the entry of lanthanum into the calcite lattice is not observed.

It can be concluded based on the study of the morphology of lanthanum and indium orthoborates that the phases of aragonite $La_{0.98}Eu_{0.02}BO_3$ and calcite $In_{0.98}Eu_{0.02}BO_3$ contain microcrystals of size $1-6\,\mu$m and $\sim 1\,\mu$m and less, respectively. Two-phase samples contain both particle fractions of different dispersion with quantities correlating with the ratio of lanthanum and indium.

It was shown that indium and lanthanum orthoborates do not form joint solid solutions.

Acknowledgments

The authors thank the Research Facility Center of ISSP RAS for the morphology study of the samples and their characterization by IR spectroscopy and X-ray diffraction analysis methods.

Funding

The research is carried out within the state task of ISSP RAS.

Conflict of interest

The authors declare that they have no conflict of interest.

References

[1] E.F. Shubert, J.K. Kim. Science **308**, 1274 (2005).
[2] X. Zhang, X. Fu, J. Song, M.-L. Gong. Mater. Res. Bull. **80**, 177 (2016).
[3] C. Mansuy, J.M. Nedelec, C. Dujardin, R. Mahiou. Opt. Mater. **29**, 6, 697 (2007).
[4] J.-P. Meyu, T. Jensen, G. Huber. IEEE J. Quantum Electron 30:913 (1994).
[5] D. Lu, Z. Pan, H. Zwang, J. Wang. Opt. Mater Exp. **5**, *8*, 1822 (2015).
[6] A.B. Kuznetsov, K.A. Kokh, N.G. Kononova, V.S. Shevchenko, S.V. Rashchenko, D.M. Ezhov, A.Y. Jamous, A. Bolatov, B. Uralbekov, V.A. Svetlichnyi, A.E. Kokh. J. Alloys Comp. **851**, 156825 (2021).
[7] V.V. Mikhailin, D.A. Spassky, V.N. Kolobanov, A.A. Meotishvili, D.G. Permenov, B.I. Zadneprovski. Rad. Measurem. **45**, 307 (2010).
[8] J. Yang, G. Zhang, L. Wang, Z. You, S. Huang, H. Lian, J. Lin. J. Solid State Chem. **181**, 2672 (2008).
[9] G. Blasse, Grabmaier B.C. Luminescent Materials. Springer–Verlag, Berlin–Heiderberg (1994). 233 p.
[10] Jun Yang, Chunxia Li, Xiaoming Zhang, Zewei Quan, Cuimiao Zhang, Huaiyong Li, Jun Lin. Chem. Eur. J. **14**, *14*, 4336 (2008).
[11] S.Z. Shmurak, V.V. Kedrov, A.P. Kiselev, I.M. Shmyt'ko, FTT **57**, *1*, 19 (2015). (in Russian).
[12] S.Z. Shmurak, V.V. Kedrov, A.P. Kiselev, T.N. Fursova, I.M. Shmytko, FTT **57**, *8*, 1558 (2015). (in Russian).
[13] S.Z. Shmurak, V.V. Kedrov, A.P. Kiselev, T.N. Fursova, I.I. Zver'kova, E.Yu. Postnova, FTT **63**, *7*, 933 (2021). (in Russian).
[14] S.Z. Shmurak, V.V. Kedrov, A.P. Kiselev, T.N. Fursova, I.I. Zver'kova, E.Yu. Postnova, FTT **63**, *10*, 1615 (2021). (in Russian).
[15] S.Z. Shmurak, V.V. Kedrov, A.P. Kiselev, T.N. Fursova, I.I. Zver'kova, FTT **62**, *12*, 2110 (2020). (in Russian).
[16] J. Hö lsä. Inorg. Chim. Acta **139**, *1–2*, 257 (1987).
[17] E.M. Levin, R.S. Roth, J.B. Martin. Am. Miner. **46**, *9–10*, 1030 (1961).
[18] G. Chadeyron, M. El-Ghozzi, R. Mahiou, A. Arbus, C. Cousseins. J. Solid State Chem. **128**, 261 (1997).
[19] .D. Santamaría-Pérez, O. Gomis, J. Angel Sans, H.M. Ortiz, A. Vegas, D. Errandonea, J. Ruiz-Fuertes, D. Martinez-Garcia, B. Garcia-Domene, André L.J. Pereira, F. Javier Manjón, P. Rodríguez-Hernández, A. Muñoz, F. Piccinelli, M. Bettinelli, C. Popescu. J. Phys. Chem. C **118**, 4354 (2014).
[20] Wen Ding, Pan Liang, Zhi-Hong Liu. Mater. Res. Bull. **94**, 31 (2017).
[21] Wen Ding, Pan Liang, Zhi-Hong Liu. Solid State Sci. **67**, 76 (2017).
[22] S.Z. Shmurak, V.V. Kedrov, A.P. Kiselev, T.N. Fursova, I.I. Zver'kova, S.S. Khasanov, FTT **63**, *12*, 2142 (2021). (in Russian).
[23] N.I. Steblevskaya, M.I. Belobeletskaya, M.A. Medkov. Zhurn. neorgan. khimii **66**, *4*, 440 (2021). (in Russian).
[24] J. Guang, C. Zhang, C. Wang, L. Liu, C. Huang, S. Ding. Cryst. Eng. Commun. **14**, 579 (2012).
[25] J. Zhang, M. Yang, H Jin, X. Wang, X. Zhao, X. Liu, L. Peng. Mater. Res. Bull. **47**, 247 (2012).
[26] S.Z. Shmurak, V.V. Kedrov, A.P. Kiselev, T.N. Fursova, I.I. Zver'kova, FTT **64**, *8*, 955 (2022). (in Russian).
[27] S.Z. Shmurak, V.V. Kedrov, A.P. Kiselev, T.N. Fursova, I.I. Zver'kova, FTT **64**, *12*, 2000 (2022). (in Russian).
[28] S.Z. Shmurak, V.V. Kedrov, A.P. Kiselev, T.N. Fursova, I.I. Zver'kova, FTT **64**, *4*, 474 (2022). (in Russian).
[29] S.Z. Shmurak, V.V. Kedrov, A.P. Kiselev, T.N. Fursova, I.I. Zver'kova, FTT **65**, *2*, 312 (2023). (in Russian).
[30] Heng-Wei Wei, Li-Ming Shao, Huan Jiao, Xi-Ping Jing. Opt. Mater. **75**, 442 (2018).
[31] R. Nayar, S. Tamboli, A.K. Sahu, V. Nayar, S.J. Dhoble. J. Fluoresc. **27**, 251 (2017).
[32] S.K. Omanwar, N.S. Savala. Appl. Phys. A **123**, 673 (2017).
[33] A. Haberer, R. Kaindl, H. Huppertz. Z. Naturforsch. B **65**, 1206 (2010).
[34] R. Velchuri, B.V. Kumar, V.R. Devi, G. Prasad, D.J. Prakash, M. Vital. Mater. Res. Bull. **46**, *8*, 1219 (2011).
[35] Jin Teng-Teng, Zhang Zhi-Jun, Zhang Hui, Zhao Jing-Tai. J. Inorganic Mater. **28**, *10*, 1153 (2013).
[36] K.K. Palkina, V.G. Kuznetsov, L.A. Butman, B.F. Dzhurinsky, Koordinatsionnaya khimiya **2**, *2*, 286 (1976). (in Russian).
[37] S. Lemanceau, G. Bertrand-Chadeyron, R. Mahiou, M. El-Ghozzi, J.C. Cousseins, P. Conflant, R.N. Vannier. J. Solid State Chem. **148**, 229 (1999).

[38] N. Akçamlı, D. Ağaoğulları, Ö. Balcı, M. Lütfi Öveçoğlu, İ. Duman. Ceram. Int. **42**, 10045 (2016).
[39] C.E. Weir, E.R. Lippincott. J. Res. Natl. Bur. Std. A **65**, *3*, 173 (1961).
[40] A. Szczeszak, T. Grzyb, St. Lis, R.J. Wiglusz. Dalton Transact. **41**, 5824 (2012).
[41] Ling Li, Shihong Zhou, Siyuan Zhang. Solid State Sci. **10**, 1173 (2008).
[42] S.Z. Shmurak, V.V. Kedrov, A.P. Kiselev, T.N. Fursova, I.I. Zver'kova, FTT **65**, *5*, 822 (2023). (in Russian).
[43] D.A. Keszler, H. Sun. Acta Crystallogr. C **44**, 1505 (1988).
[44] A.G. Ryabukhin, Izv. Chelyabinskogo nauch. tsentra **4**, 33 (2000). (in Russian).
[45] W.C. Steele, J.C. Decius. J. Chem. Phys. **25**, *6*, 1184 (1956).

Translated by A.Akhtyamov